Isoflurane modulates activation and inactivation gating of the prokaryotic Na$^+$ channel NaChBac

Rheanna M. Sand,[1] Kevin J. Gingrich,[3] Tamar Macharadze,[1] Karl F. Herold,[1] and Hugh C. Hemmings Jr.[1,2]

[1]Department of Anesthesiology and [2]Department of Pharmacology, Weill Cornell Medical College, New York, NY 10065
[3]Department of Anesthesiology, University of Texas Southwestern Medical Center, Dallas, TX 75235

Voltage-gated Na$^+$ channels (Na$_v$) have emerged as important presynaptic targets for volatile anesthetic (VA) effects on synaptic transmission. However, the detailed biophysical mechanisms by which VAs modulate Na$_v$ function remain unclear. VAs alter macroscopic activation and inactivation of the prokaryotic Na$^+$ channel, NaChBac, which provides a useful structural and functional model of mammalian Na$_v$. Here, we study the effects of the common general anesthetic isoflurane on NaChBac function by analyzing macroscopic Na$^+$ currents (I_{Na}) in wild-type (WT) channels and mutants with impaired (G229A) or enhanced (G219A) inactivation. We use a previously described six-state Markov model to analyze empirical WT and mutant NaChBac channel gating data. The model reproduces the mean empirical gating manifest in I_{Na} time courses and optimally estimates microscopic rate constants, valences (z), and fractional electrical distances (x) of forward and backward transitions. The model also reproduces gating observed for all three channels in the absence or presence of isoflurane, providing further validation. We show using this model that isoflurane increases forward activation and inactivation rate constants at 0 mV, which are associated with estimated chemical free energy changes of approximately −0.2 and −0.7 kcal/mol, respectively. Activation is voltage dependent ($z \approx 2e_0$, $x \approx 0.3$), inactivation shows little voltage dependence, and isoflurane has no significant effect on either. Forward inactivation rate constants are more than 20-fold greater than backward rate constants in the absence or presence of isoflurane. These results indicate that isoflurane modulates NaChBac gating primarily by increasing forward activation and inactivation rate constants. These findings support accumulating evidence for multiple sites of anesthetic interaction with the channel.

INTRODUCTION

With over 170 years of clinical use since the public demonstration of general anesthesia, the molecular mechanisms of general anesthetic drugs are still not fully understood (Hemmings et al., 2005; Franks, 2006). It is widely accepted that general anesthetics alter neuronal signaling by interacting with membrane proteins, in particular ligand-gated ion channels, rather than with the lipid bilayer (Herold et al., 2017). More recent evidence suggests that voltage-gated ion channels, including presynaptic voltage-gated Na$^+$ channels (Na$_v$), are important targets for anesthetic ethers (Franks, 2006; Herold and Hemmings, 2012). Several mammalian isoforms of Na$_v$, which in neurons drive the upstroke of the action potential and act upstream of neurotransmitter release, are inhibited by the common volatile anesthetic (VA) isoflurane (Rehberg et al., 1996; Shiraishi and Harris, 2004; OuYang and Hemmings, 2007; Herold et al., 2009, 2014; for review, see Herold and Hemmings, 2012). However, the mechanisms by which VAs such as isoflurane inhibit Na$_v$ remain unresolved.

Homologous bacterial voltage-gated Na$^+$ channels have emerged as useful structural and functional models for the more complex mammalian Na$_v$ (Catterall and Zheng, 2015; Payandeh and Minor, 2015). The

prokaryotic channels are expressed as monomers that form homotetrameric channels (in contrast to the four contiguous pore-forming domains of mammalian Na$_v$ α-subunits), making them more amenable to heterologous expression, mutagenesis, and x-ray crystallography (Payandeh et al., 2011, 2012; McCusker et al., 2012; Zhang et al., 2012; Shaya et al., 2014). Prokaryotic Na$_v$ lack the fast-inactivation particle found in eukaryotic Na$_v$ but exhibit slow inactivation similar to eukaryotic Na$_v$ (Kuzmenkin et al., 2004; Pavlov et al., 2005; Irie et al., 2010), such that prokaryotic Na$_v$ homologues are particularly useful in isolating pharmacological effects on slow inactivation.

NaChBac, the voltage-gated Na$^+$ channel from *Bacillus halodurans* (Ren et al., 2001), is modulated by isoflurane (Ouyang et al., 2007) and sevoflurane (Barber et al., 2014). Isoflurane reduces peak Na$^+$ current (I_{Na}) at more depolarized holding potentials, shifts the steady-state inactivation (SSI) curve in the hyperpolarizing direction, and accelerates apparent inactivation, which was interpreted as preferential binding to an inactivated state (Ouyang et al., 2007). In contrast, modeling studies have suggested that sevoflurane inhibits NaChBac by

Correspondence to Hugh C. Hemmings Jr.: hchemmi@med.cornell.edu
Abbreviations used: LA, local anesthetic; NMR, nuclear magnetic resonance; SSI, steady-state inactivation; VA, volatile anesthetic.

slow open channel block with no effect on inactivation kinetics (Barber et al., 2014). Despite these different proposed mechanisms of action, the structurally similar halogenated ethers isoflurane and sevoflurane have similar effects on Na$_v$1.4 (Ouyang et al., 2009). Of interest, molecular dynamics simulations have identified multiple sites of interaction for both isoflurane (Raju et al., 2013) and sevoflurane (Barber et al., 2014) with NaChBac, including the pore cavity and fenestrations, S4–S5 linker, activation gate, and selectivity filter. Recently, binding of isoflurane to NaChBac was identified using ^{19}F nuclear magnetic resonance (^{19}F NMR; Kinde et al., 2016). Strong interactions were found with the S4–S5 linker, an extracellular pore loop, and the base of the selectivity filter, which were postulated as sites involved in channel inhibition. To validate these computational and structural findings and better understand Na$_v$ modulation by anesthetic ethers, functional electrophysiological analyses are paramount. Previous functional studies showed that isoflurane accelerates activation (Ouyang et al., 2007), an effect not addressed in previous computational and structural studies, and it is possible that anesthetic-induced changes in macroscopic inactivation arise indirectly through altered activation (Aldrich et al., 1983).

We therefore investigated isoflurane effects on the electrophysiological properties of WT NaChBac and NaChBac mutated to alter activation and inactivation. We analyzed our empirical electrophysiological data using a recognized Markov model of NaChBac gating (Kuzmenkin et al., 2004) to resolve isoflurane effects on discrete gating parameters and better discern its mechanisms of action. Our results indicate that the primary effects of isoflurane on NaChBac gating include enhancement of both forward activation and inactivation rate constants that arise from the reduction of associated free energy barriers, and do not favor slow open channel block.

MATERIALS AND METHODS

NaChBac constructs
WT NaChBac cDNA (from *B. halodurans*) in a modified pTracer expression vector with a GFP-Zeocin site (Invitrogen) was provided by D. Clapham (Harvard University, Boston, MA). NaChBac slow inactivation was modified by introducing two known point mutations in the S6 helix at the so-called gating hinge: G219A accelerates and G229A slows inactivation, respectively (Irie et al., 2010). Site-directed mutagenesis was performed using the QuikChange II kit (Agilent Technologies). The entire open reading frames of successful cDNA clones were confirmed by sequencing.

Electrophysiology
Mammalian HEK293FT cells (Invitrogen) were maintained in high-glucose Dulbecco's modified Eagle medium supplemented with 1% penicillin-streptomycin, 500 µg/ml geneticin, 6 mM GlutaMAX (Invitrogen), 1 mM sodium pyruvate, 0.1 mM nonessential amino acids, and 10% (vol/vol) FBS; passage numbers between 3 and 30 were used. Cells were seeded into a 24-well plate and transfected with the respective NaChBac cDNA, as well as eGFP-N1 as a reporter plasmid, on the next day using Lipofectamine LTX (Invitrogen) according to the manufacturer's protocol. At day 1–2 after transfection, cells were released with trypsin and replated onto 12-mm round #1.5 glass coverslips (Warner Instruments) a minimum of 1 h before recording isolated adherent cells with GFP fluorescence.

Pipettes were pulled from standard borosilicate glass (1.5 mm OD/0.86 mm ID; Sutter Instrument) to a resistance of 1.5–2.8 MΩ (when filled) using a P97 puller (Sutter Instrument) and fire polished. Whole-cell voltage-clamp was performed using an AxoPatch 200B amplifier (Molecular Devices) connected to a DigiData 1320A analogue-to-digital converter (Molecular Devices). Signals were sampled at 10 or 20 kHz and filtered at 2 or 5 kHz, respectively. Series resistance was corrected 75–80%. Capacitive current transients were cancelled by the internal amplifier circuitry, and leak currents were subtracted using a standard P/4 protocol.

Cells were continuously perfused with extracellular solution at room temperature (22–23°C) containing (mM) 140 NaCl, 10 Hepes, 3 KCl, 1.8 CaCl$_2$, 1 MgCl$_2$, and 10 tetraethylammonium chloride (TEA-Cl), adjusted to pH 7.35 with NaOH. Osmolality was 307 mOsm/kgH$_2$O. Pipette solutions contained (mM) 120 CsF, 10 NaCl, 10 Hepes, 10 ethylene glycol tetraacetic acid, 10 TEA-Cl, 1 MgCl$_2$, and 1 CaCl$_2$, adjusted to pH 7.30 with CsOH and to 310 mOsm/kgH$_2$O with sucrose. Saturated isoflurane (Abbott Laboratories) stock solutions were prepared in extracellular solution in gas-tight glass vials. Dilutions in gas-tight syringes were delivered using a pressurized perfusion system (ALA Scientific Instruments) with Teflon tubing, via a 200-µm-diameter manifold tip positioned ∼200–300 µm from the recorded cell. After control recordings, isoflurane was perfused for 2 min before subsequent recordings and continuously thereafter until washout. Solutions were delivered through a pressurized perfusion system to minimize mechanical disturbance of cells during isoflurane superfusion. Mock experiments with extracellular solution showed no effect on I_{Na}. Working solutions of 0.8 mM isoflurane, a clinically effective concentration in mammals equivalent to about twice the minimum alveolar concentration (Taheri et al., 1991), were confirmed by gas chromatography (Herold et al., 2009).

Data analysis
Voltage-clamp data were collected and analyzed using pCLAMP v10.2 (Molecular Devices), with additional data processing and analysis using Prism v5.01 (Graph-
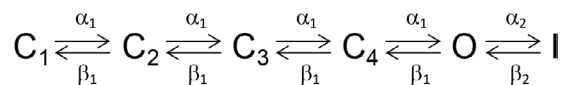
Pad Software) and Excel 2010 and 2013 (Microsoft). Differences between groups were assessed using Student's t test except for fitted curves (i.e., conductance-voltage, concentration-response, and SSI), for which certain parameters were compared using an F test. In all cases, statistical significance was defined as $P < 0.05$. Data are reported as mean ± SEM. Confidence of estimated model parameters are reported with 95% confidence intervals.

Currents were converted to conductance (G) using $G = I/[V - V_{rev}]$, where I is the measured current, V is the command potential, and V_{rev} is the reversal potential derived from linear extrapolations of individual current-voltage (I-V) curves. Voltage dependence of activation was quantified by first relating peak conductance (G) normalized by the maximum G (G_{max}) to the pulse potential, which was followed by a quantitative description of this relation using a two-state Boltzmann equation of the form $G/G_{max} = 1/\big[1 + e^{(V-V_{50})/k}\big]$, where V is voltage, V_{50} is the midpoint voltage, and k is the slope factor. SSI curves were fitted in a similar fashion. Concentration–response relations of peak current were fitted with a logistic equation of the form $Y = 1/(1 + IC_{50}/[ISO]^{slope})$, where Y is the response variable, $[ISO]$ is the isoflurane concentration, IC_{50} is the isoflurane concentration at 50% inhibition, and $slope$ is a factor related to the Hill coefficient. Response time courses were fitted with a time-shifted biexponential function: $\big[A_1 e^{-(t-t_s)/\tau_1} + A_2 e^{-(t-t_s)/\tau_2} + B\big]$, where A_n is the nth component amplitude, B is a constant representing a plateau, t is time, t_S is the time shift, and τ_n is the nth component time constant. Function values before t_S were set to zero.

Kinetic modeling

Na_v exhibits at least three conformational states: closed (C) before channel opening, open (O) conducting states triggered by depolarization, and inactivated (I) closed states visited after activation. The macroscopic Na^+ current (I_{Na}) time course can be viewed as: $I_{Na}(t) = [\gamma(V - V_{rev})]nP_o(t,V)$, where t is time, V is membrane voltage, V_{rev} is the reversal potential, γ is single-channel conductance, n is channel number, and P_o is the time course of the single-channel open probability. We collected I_{Na} families over a range of triggering voltages (−40 to 0 mV) for each channel in the absence and presence of isoflurane. Currents were then adjusted for driving force, resulting in responses reporting $\gamma nP_o(t)$ at each voltage and normalized to the peak of the 0-mV response in control (or in isoflurane if it was greater) to yield families reporting $[P_o(t,V)/Peak\ P_o(t, 0\ mV)]$. This normalized P_o can be analyzed to gain insight into the underlying gating and the effects of isoflurane.

Kuzmenkin et al. (2004) proposed a six-state Markov model of NaChBac gating based and validated on the results of ionic and gating current analysis (see Scheme 1):

$$C_1 \underset{\beta_1}{\overset{\alpha_1}{\rightleftharpoons}} C_2 \underset{\beta_1}{\overset{\alpha_1}{\rightleftharpoons}} C_3 \underset{\beta_1}{\overset{\alpha_1}{\rightleftharpoons}} C_4 \underset{\beta_1}{\overset{\alpha_1}{\rightleftharpoons}} O \underset{\beta_2}{\overset{\alpha_2}{\rightleftharpoons}} I$$

(Scheme 1)

In this model, the pore is presumed to be controlled by four activation gates, one contributed by each of the four component homomeric subunits, and all are required to be activated to reach the open conducting state (O). Each transition starting from C_1 represents the opening of one of the activation gates until the final is opened upon transition from C_4 to O. These transitions are governed by identical forward (α_1) and backward (β_1) rate constants such that each subunit's conformational transitions are identical and independent. Once open, O can then transition to the inactivated state (I) governed by forward (α_2) and backward (β_2) rate constants. The voltage dependence of forward and backward transition rates is given by $\alpha_1(V) = k_{\alpha_1}(0) e^{(z_1 x_1 FV/RT)}$ and $\beta_1(V) = k_{\beta_1}(0) e^{[-z_1(1-x_1)FV/RT]}$ for activation and by $\alpha_2(V) = k_{\alpha_2}(0) e^{(z_2 x_2 FV/RT)}$ and $\beta_2(V) = k_{\beta_2}(0) e^{(-z_2(1-x_2)FV/RT)}$ for inactivation, where $k_{\alpha1}(0)$, $k_{\beta1}(0)$, $k_{\alpha2}(0)$, and $k_{\beta2}(0)$ are transition rate constants at 0 mV; z_1 and z_2 are the valences of activation and inactivation transitions; x_1 and x_2 are fractions of the electric field where the energy barrier peak is located for activation and inactivation, respectively; V is membrane voltage; F is the Faraday constant; R is the universal gas constant; and T is absolute temperature. Solutions to the associated differential equations of the six-state Markov model were obtained using MATLAB v7.5 (MathWorks) by solving the matrix equation $X(t) = e^{Q(t)}X(0)$, where $X(t)$ is a 6×1–state variable vector reporting the probability of C_1 to C_4, O, and I states at time t; $X(0)$ is the initial state vector at time 0; and $Q(t)$ is the 6×6–state transition matrix of rate constants governing the transition rates between all connected states. We used the Levenberg–Marquardt method (MATLAB Optimization Toolbox 4.1; MathWorks) to solve iteratively for a set of parameters, $k_{\alpha1}(0)$, $k_{\beta1}(0)$, $k_{\alpha2}(0)$, $k_{\beta2}(0)$, z_1, z_2, x_1, and x_2, and scaling factors, K_{-40mV} to K_{0mV}, that provides a best fit to a family of mean normalized P_o time courses obtained over a range of voltages (−40 to 0 mV). Scaling factors (K_{-40mV} to K_{0mV}) were applied to model responses at the indicated voltage to account for the nature of normalized P_o responses, the influence of model parameters on peak probability of state O, and experimental variability. During parameter estimation, z and x values were limited to ranges of 0 to $5e_0$ and 0 to 1, respectively. All other parameters were limited to positive values. This process resulted in a set of parameter values for each voltage family of mean normalized P_o responses for each channel

and condition. 95% confidence intervals of estimated parameters were calculated.

Estimation of free energy changes in gating transitions modulated by isoflurane

Eyring rate theory (Eyring, 1935) holds that a gating transition rate is determined by the energy barrier height that must be overcome to transition from one kinetic state to another and is described by $\Delta G = -RT\ln[k_{ij}(0)/(\kappa k_B T/h)]$, where $k_{ij}(0)$ is the rate constant governing transitions from state i to j at zero membrane voltage, ΔG is the height of the free energy barrier for this transition, κ is the transmission coefficient (assumed to be 1), k_B is Boltzmann's constant, h is Planck's constant, and R and T are the same as above. Therefore, the change in ΔG induced by isoflurane (ΔG_{ISO}) is obtained by determining the difference between ΔG in CTL and ISO, such that $\Delta G_{ISO} = -RT\ln[k_{ij}(0)_{ISO}/k_{ij}(0)_{CTL}]$, where $k_{ij}(0)_{ISO}$ and $k_{ij}(0)_{CTL}$ are obtained as described above.

RESULTS

Effect of isoflurane on NaChBac voltage-dependent activation

Expression of WT NaChBac in HEK293FT cells produced robust whole-cell Na^+ currents (I_{Na}; Fig. 1 A, left) that were not observed in sham-transfected cells (not depicted). Control I_{Na} collected over a range of depolarizing potentials and the associated current-voltage (*I-V*) and normalized conductance-voltage (*G-V*) relationships (Fig. 1, left) agree with previous studies of NaChBac (Ren et al., 2001; Ouyang et al., 2007). Isoflurane (0.8 mM) effects, collected from the same cells as control, showed accelerated I_{Na} decay, with the rising phase of the *I-V* relationship shifted to the left without reduced peak I_{Na}, indicating enhanced apparent inactivation and altered voltage-dependent activation, respectively. Fitting of *G-V* relationships revealed significant reduction in V_{50}, further supporting altered activation (Fig. 1 C).

Isoflurane acceleration of apparent I_{Na} inactivation (see Fig. 4, left) could be explained by promotion of the inactivated state (Ouyang et al., 2007), or alternatively by slow block of open channels (Barber et al., 2014). To begin to discriminate between these mechanisms, we studied NaChBac channels with G229A and G219A mutations that slow or accelerate inactivation, respectively (Irie et al., 2010). In control conditions, current decay was slowed in G229A and accelerated in G219A relative to WT (Fig. 1 A, middle and right), consistent with a previous study (Irie et al., 2010). Isoflurane (0.8 mM) accelerated current decay in both G229A and G219A similar to WT (Fig. 1 A). The current peak of *I-V* relationships was slightly increased by isoflurane in G229A but markedly reduced (by ~50%) in G219A (Fig. 1 B). Fitting of the G219A *G-V* relationship showed a hyper-

polarizing shift of V_{50} similar to that of WT, which was not observed for G229A.

Isoflurane qualitatively accelerated apparent inactivation irrespective of the control inactivation rate, which argues against a simple open channel blocking mechanism. Furthermore, isoflurane induced a leftward shift of the *G-V* relationship, indicating a relative stabilization of the open state in WT and G219A. These findings point to direct effects of isoflurane on both activation and inactivation.

Concentration dependence of isoflurane effects on peak current

The concentration dependence of isoflurane effects was investigated by delivering single depolarizing pulses to −10 mV after exposure to increasing concentrations of isoflurane, with a maximum of three concentrations tested per cell (Fig. 2). Pulses were also delivered after isoflurane washout to ensure that peak currents had returned to control levels at the end of the experiment. In contrast to the results obtained in *I-V* plots (Fig. 1), a slight peak current reduction was observed for WT NaChBac at 0.8 mM isoflurane. In all three channels, most strikingly in G219A, isoflurane depressed peak I_{Na} in a concentration-dependent manner. G229A current amplitudes were slightly increased at 0.8 mM, similar to results shown in Fig. 1, but were reduced at higher concentrations. IC_{50} values obtained from logistic curve fits suggest differential sensitivities (G219A > WT > G229A), consistent with the results in Fig. 1. The differences in IC_{50} were statistically significant across all three groups. Isoflurane also enhanced I_{Na} decay rate in a concentration-dependent manner in all three channels.

Isoflurane effects on inactivation

Inactivation recovery time courses were well fitted by a biexponential function for all channels (Fig. 3 A), consistent with both slow and fast inactivated states. The slow time constant (τ_S) agrees with the monoexponential recovery reported for longer conditioning depolarizations (Ren et al., 2001). Isoflurane accelerated WT channel recovery from inactivation by increasing the fast component amplitude (A_F) at the expense of the slow (A_S) without changes in time constants (Fig. 3 A, left, inset). Isoflurane failed to alter G219A inactivation recovery, as indicated by superimposable control and isoflurane responses (Fig. 3 A, right). For G229A, test pulse durations failed to inactivate all channels in control. Isoflurane enhanced inactivation, leading to a greater fraction of inactivated channels. However, a scaled version of the isoflurane response reproduced the control response (Fig. 3 A, middle), indicating that isoflurane failed to change recovery time constants and relative amplitudes of the two exponential components.

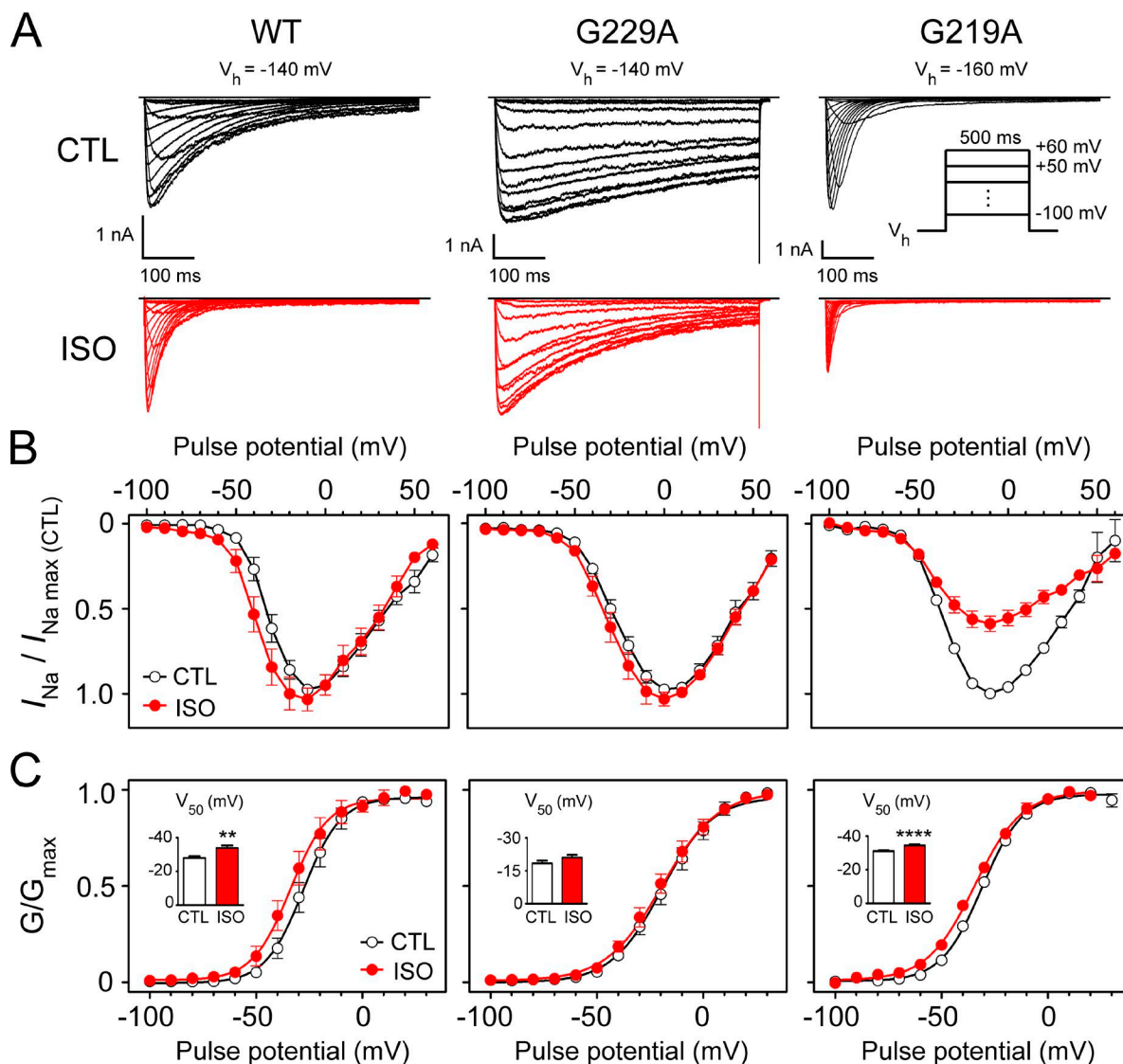We next examined the onset kinetics of current inactivation (Fig. 3 B). Because conditioning pulses lasting

Figure 1. **Isoflurane effects on voltage-dependent gating.** (A) Representative families of macroscopic I_{Na} in the absence (CTL) or presence of 0.8 mM isoflurane (ISO), elicited from HEK293FT cells expressing WT NaChBac or the mutant forms G229A and G219A as indicated. Inset shows triggering voltage-clamp protocol (stimulation frequency, 0.167 Hz; V_h, holding potential). G229A tail currents clipped for clarity. Horizontal black lines indicate baseline; calibration bars as shown. (B) Normalized I-V relationships for each channel. Currents normalized by peak current in control for each cell ($n = 5$–6). (C) Normalized G-V relationships in CTL and 0.8 mM ISO. Conductance (G) normalized by maximum conductance (G_{max}) and plotted versus voltage. Smooth lines are Boltzmann function fits to the averaged data with associated parameters (V_{50}, voltage at half amplitude; slope factor: WT, $V_{50(CTL)} = -28.0 \pm 1.0$ mV, $V_{50(ISO)} = -33.8 \pm 1.5$ mV, slope$_{CTL} = 8.4 \pm 0.9$ mV/e, slope$_{ISO} = 9.6 \pm 1.3$ mV/e; G229A, $V_{50(CTL)} = -18.4 \pm 1.3$ mV, $V_{50(ISO)} = -21.0 \pm 1.2$ mV, slope$_{CTL} = 12.0 \pm 1.1$ mV/e, slope$_{ISO} = 12.8 \pm 1.1$ mV/e; G219A, $V_{50(CTL)} = -31.1 \pm 0.5$ mV, $V_{50(ISO)} = -34.5 \pm 0.7$ mV, slope$_{CTL} = 9.5 \pm 0.4$ mV/e, slope$_{ISO} = 11.1 \pm 0.6$ mV/e). Asterisks indicate differences between CTL and ISO fits with respect to V_{50} only (**, P < 0.01; ****, P < 0.0001; F test). Isoflurane significantly altered the slope factor of G219A alone (P = 0.028; F test). All error bars represent SEM.

minutes are required to reach steady state (Pavlov et al., 2005), we determined the minimum conditioning pulse duration needed for SSI protocols. These protocols did not address onset kinetics at a range of conditioning voltages and thus were not intended to be an exhaustive examination of isoflurane effects on onset kinetics.

Onset time courses were characterized at control holding potentials and at potentials of 40 mV more positive.

The latter was chosen based on preliminary data indicating a threshold of SSI curves near these voltages. For all three channels, little inactivation was observed for control conditions, whereas isoflurane decreased channel availability monoexponentially with V_{pre} duration. WT and G219A time constants were <20 s, in contrast to 60 s for G229A, with steady-state conditions reached in ~60 s and ~200 s, respectively, assuming three time
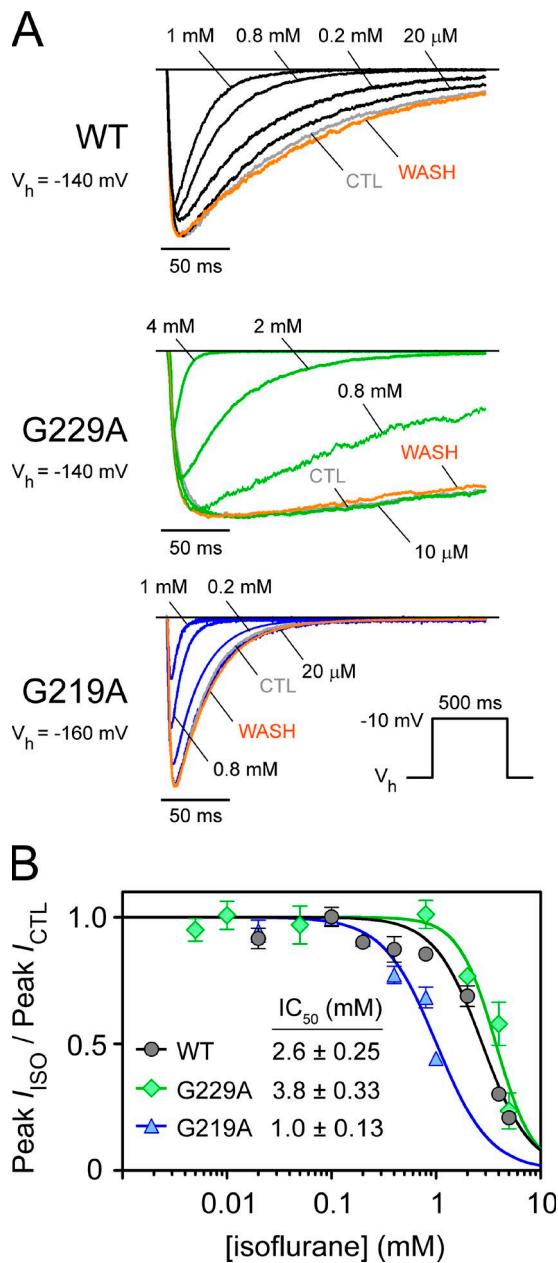
A

WT
V_h = -140 mV

G229A
V_h = -140 mV

G219A
V_h = -160 mV

B

Figure 2. **Concentration dependence of isoflurane peak I_{Na} inhibition.** (A) Representative normalized I_{Na} time courses over a range of isoflurane (ISO) concentrations (indicated) for WT, G229A, and G219A. Individual I_{Na} responses obtained from a single cell exposed to ISO with initial control (CTL) and bracketing washout (WASH) are shown; other concentrations were obtained from individual cells. Responses are normalized to peak I_{Na} in CTL. Horizontal black lines indicate baseline. Inset shows voltage protocol (frequency, 0.167 Hz; V_h, holding potential). (B) Concentration-response relationships for peak I_{Na} inhibition for each channel. Peak I_{Na} in isoflurane (Peak I_{ISO}) was normalized by that of control (Peak I_{CTL}) and plotted versus isoflurane concentration (n = 3–10; mean ± SEM). Curves are logistic function fits with indicated IC_{50} values, which were significantly different across all three channels (P < 0.0001; F test).

constants to steady state. SSI protocols involving 200-s pulses were prohibitively long, and therefore data for G229A SSI were not obtained.

Data for WT and G219A SSI were collected using a three-pulse protocol with a 90-s conditioning pulse (Fig. 3 C). Preparation stability provided data for up to three voltages per cell, and results from multiple cells were then combined to create SSI curves. Isoflurane shifted SSI curves in the hyperpolarized direction, reducing V_{50} by ~16 mV and ~25 mV for WT and G219A, respectively, with little change in Boltzmann slope factors. The results indicate that isoflurane induces a relative stabilization of the inactivated states.

Kinetic analysis of current time course

Isoflurane qualitatively accelerated activation and inactivation in WT NaChBac, consistent with previous findings (Ouyang et al., 2007), as well as in both mutant channels (Fig. 4 A). We analyzed isoflurane-induced changes in activation and inactivation kinetics using a biexponential function with rising and falling components to provide initial quantitative insight into channel gating (see Materials and methods). Biexponential function fits reproduced the time course of all channels in control and isoflurane, with the exception of the initial activation phase occurring in the first few milliseconds (Fig. 4 B, arrow), likely arising from channel transitions through multiple closed states before opening (Kuzmenkin et al., 2004). Compared with WT, G229A and G219A mutations slowed or accelerated inactivation (τ_{inact}), respectively, but neither mutation significantly altered activation kinetics (τ_{act}; Fig. 4 C). Isoflurane effects on associated time constants indicate acceleration of activation and inactivation for all three channels.

Gating analysis using the six-state Markov model

Macroscopic rates are a function of both microscopic rate constants and relevant channel state probabilities. To gain insight into microscopic gating, we applied a previously described six-state Markov model of NaChBac gating (Kuzmenkin et al., 2004) to our experimental results (Fig. 5 A). Because I_{Na} is proportional to probability of model state O (model P_o), we transformed current time courses into normalized open channel probability (normalized P_o; see Materials and methods). We then calculated mean normalized P_o responses (Fig. 5 B). Fitting model P_o responses to a family of mean normalized P_o responses obtained over a range of voltages (−40 to 0 mV) involved estimation of a single set of optimal values for $k_{\alpha1}(0)$, $k_{\beta1}(0)$, $k_{\alpha2}(0)$, $k_{\beta2}(0)$, z_1, z_2, x_1, and x_2 and scaling factors K_{-40mV} to K_{0mV} (see Materials and methods). After parameter estimation, model P_o responses reproduced families of mean normalized P_o for all channels in the absence or presence of isoflurane, including the initial activation phase (Fig. 5 B),
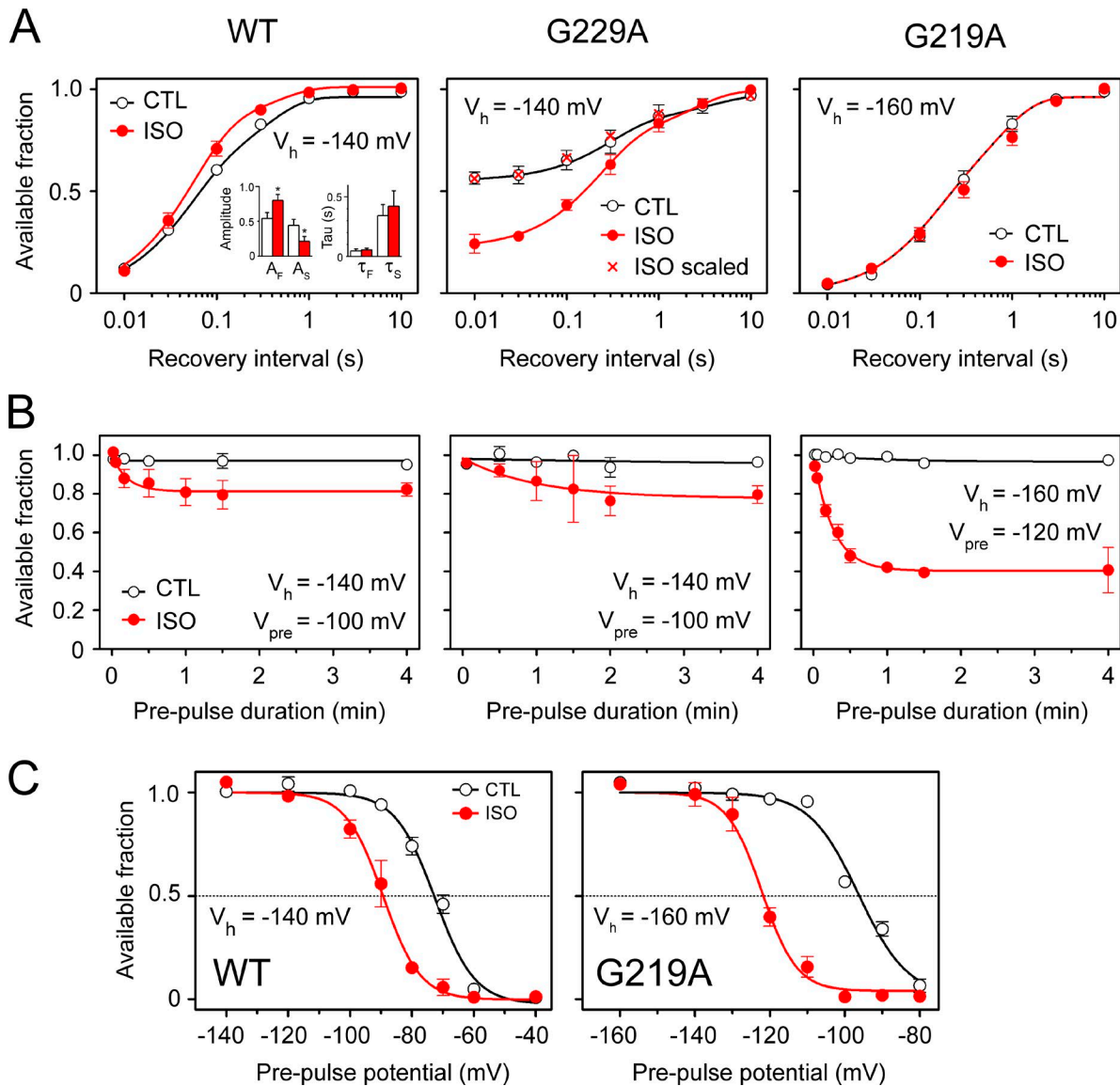
Figure 3. **Isoflurane effects on current inactivation.** (A) A two-pulse voltage protocol was used to characterize the recovery time course from inactivation. Cells were held at the indicated holding potential (V_h), and two 500-ms test pulses to -10 mV were delivered separated by a range of recovery intervals at V_h (protocol delivery frequency, <0.1 Hz). Available fractional current (peak current amplitude of pulse 2/peak amplitude of pulse 1) was plotted against recovery interval for control (CTL) and isoflurane (ISO; $n = 3$–7; mean ± SEM). Curves are biexponential fits of recovery responses: WT (CTL, $A_F = -0.57 \pm 0.063$, $\tau_F = 47 \pm 6.3$ ms, $A_S = -0.41 \pm 0.063$, $\tau_S = 320 \pm 60$ ms, B = 0.98 ± 0.006; ISO, $A_F = -0.8 \pm 0.08$, $\tau_F = 54 \pm 7$ ms, $A_S = -0.21 \pm 0.08$, $\tau_S = 400 \pm 200$ ms, B = 1.0 ± 0.01); G229A (CTL, $A_F = -0.29 \pm 0.034$, $\tau_F = 300 \pm 56$ ms, $A_S = -0.14 \pm 0.027$, $\tau_S = 3,700 \pm 2,400$ ms, B = 0.98 ± 0.02; ISO, $A_F = -0.53 \pm 0.044$, $\tau_F = 220 \pm 29$ ms, $A_S = -0.25 \pm 0.042$, $\tau_S = 2,300 \pm 720$ ms, B = 0.99 ± 0.015); G219A (CTL and ISO, $A_F = -0.4 \pm 0.082$, $\tau_F = 110 \pm 28$ ms, $A_S = -0.58 \pm 0.083$, $\tau_S = 680 \pm 105$ ms, B = 0.98 ± 0.01). G229A ISO response is also shown scaled to the same amplitude as CTL. Inset is a bar graph showing the amplitude and time constants from the WT biexponential fit for control (white bars) and 0.8 mM isoflurane (red bars) with differences by paired Student's t test: *, P < 0.05 ($n = 7$). Error bars are SEM. (B) A three-pulse voltage protocol characterized the onset time course of current inactivation. Cells were held at the indicated V_h followed by pulse 1 (-10 mV, 500 ms), a variable duration prepulse (V_{pre}), pulse 2 (-10 mV, 500 ms), and after at least 10 s at V_h, pulse 3 (-10 mV, 500 ms) to confirm preparation stability. Protocol deliveries were separated by >10 s. Available fractional current was plotted against prepulse duration for CTL and ISO ($n = 3$–6; mean ± SEM). Smooth curves are monoexponential fits (time constant, τ) of onset responses (WT, $\tau_{ISO} = 16 \pm 30$ s; G229A, $\tau_{ISO} = 60 \pm 46$ s; G219A, $\tau_{ISO} = 12 \pm 46$ s). (C) SSI relationships were characterized using a variation of the three-pulse voltage protocol used in B, in which the prepulse duration was 90 s throughout; protocol deliveries were separated by >10 s. Normalized SSI curves were obtained by plotting available fractional current against prepulse potential for CTL and 0.8 mM ISO ($n = 3$–11; mean ± SEM). Curves are Boltzmann function fits to the averaged data with associated parameters (V_{50}, voltage at half amplitude; slope factor: WT, $V_{50(CTL)} = -72.6 \pm 1.3$ mV, $V_{50(ISO)} = -89.3 \pm 1.3$ mV, slope$_{CTL}$ = -6.4 ± 0.8 mV/e, slope$_{ISO}$ = -6.0 ± 1.1 mV/e; G219A, $V_{50(CTL)} = -96.6 \pm 1.4$ mV, $V_{50(ISO)} = -122.1 \pm 0.8$ mV, slope$_{CTL}$ = -6.5 ± 0.8 mV/e, slope$_{ISO}$ = -4.6 ± 1.0 mV/e). V_{50} values were significantly different between CTL and ISO fits for both WT and G219A (P < 0.0001; F test), whereas slope factors were not different.
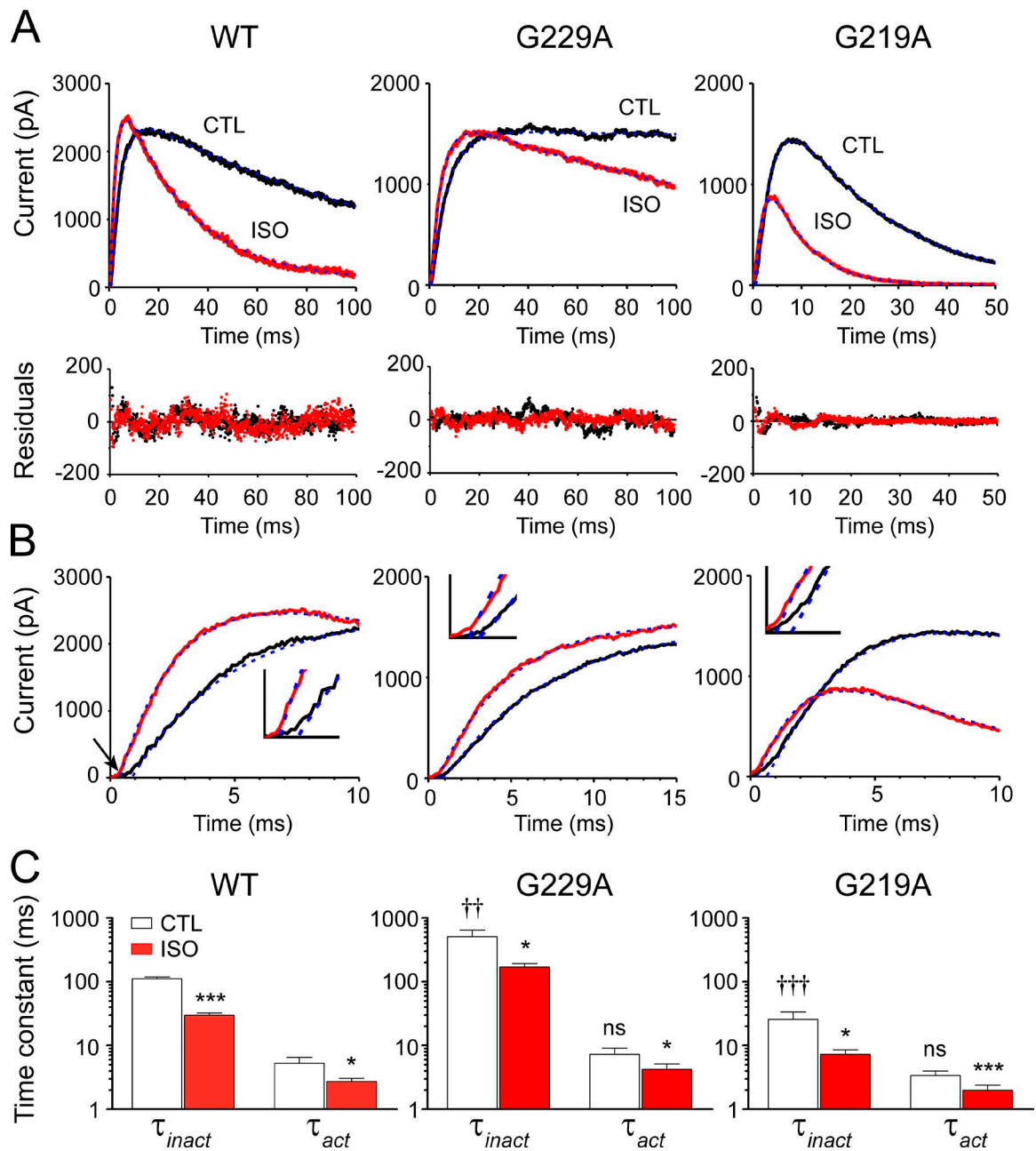
Figure 4. **Kinetic analysis of current time courses.** (A, top) Representative currents triggered by depolarization (to −10 mV using same protocol as in Fig. 1 A) for control (CTL) and 0.8 mM isoflurane (ISO) for the indicated channels. Current responses are plotted as the additive inverse. Current time courses are well described by fits of the biexponential function (dashed blue lines). In the following equations, the slower exponential is falling and describes inactivation (τ_{inact}), and the faster exponential is rising and describes activation (τ_{act}). Fitted parameters (time constant in ms): WT, I_{CTL}= 2,800 pA•[exp(−(t − 0.87)/126) − exp(−(t − 0.87)/4)], I_{ISO} = 3,300 pA•[exp(−(t − 0.39)/27) − exp(−(t − 0.39)/2.8)]; G229A, I_{CTL}= 1,570 pA•[exp(−(t − 0.86)/510) − exp(−(t − 0.86)/6.4)], I_{ISO} = 1,690 pA•[exp(−(t − 0.55)/183) − exp(−(t − 0.55)/4.6)]; G219A, I_{CTL}= 2,400 pA•[exp(−(t − 0.57)/20) − exp(−(t − 0.57)/3.4)], I_{ISO} = 1,750 pA•[exp(−(t − 0.27)/7) − exp(−(t − 0.27)/1.9); see Materials and methods. (bottom) Plots of fit residuals. (B) Responses from A replotted on an expanded timescale to focus on the early activation phase. The preponderance of the early time course is well described by the biexponential functions (dashed blue lines), except for the initial activation phase (marked by the arrow), which was not considered during biexponential function fitting; see Materials and methods. Insets show same data as in main figure plotted on an expanded timescale to show initial phase of activation time course. (C) Group time constants for inactivation (τ_{inact}) and activation (τ_{act}) phases for CTL and ISO, as indicated (n = 3–5; paired t test: *, P < 0.05; ***, P < 0.001). Control inactivation and activation time constants for G229A and G219A were also compared with WT (unpaired Student's t test: ns, not significant; ††, P < 0.01; †††, P < 0.001). Error bars are SEM.

such that this model is sufficient to account for the macroscopic gating for all channels for control or isoflurane conditions. Therefore, it is reasonable to conclude that analysis of macroscopic gating using the six-state model provides insight into isoflurane effects on microscopic gating. Rate constants derived from this analysis are proportional only to the absolute microscopic rate constants because open probabilities have not been determined. Isoflurane effects on model rate constants for a particular channel are meaningful because comparisons are made between responses from the same cell in the absence or presence of isoflurane, but comparisons between channels are not.

Estimated WT gating parameters (Fig. 6, top) for control WT NaChBac were generally similar to those of Kuzmenkin et al. (2004). $k_{\alpha 1}(0)$ and $k_{\alpha 2}(0)$ were exceptions because they are approximately threefold less, but only approximately twofold less than values reported by Barber et al. (2014). Overall, our results are comparable to those of Kuzmenkin et al. (2004), pointing to similar channel function in these preparations. The 95% confidence intervals of estimated parameters can be viewed as falling into three ranges based on the calculated fraction of the estimated parameter value: <0.15, 0.15–0.5, and >0.5, which also apply to G229A and G219A (Fig. 6, middle and bottom). The first range contains dominant model parameters that are estimated with high confidence (narrow confidence interval) and include α_1, α_2, z_1, and x_1. The second parameter confidence is less, which could be explained by smaller values of member backward rate constants (β_1 and β_2) over this voltage range. The final range comprises parameters estimated with low confidence and includes z_2 and x_2, which have large confidence intervals that include zero, suggesting that inactivation is voltage independent over this range of potentials.

Isoflurane increased WT forward rate constants of activation (α_1) and inactivation (α_2) by ~50% and ~300%, respectively, without changes in voltage dependence, and slightly reduced backward rate constants (β_1 and β_2). G229A and G219A showed similar results, except in the backward rate constant for inactivation, β_2. In G229A, β_2 was nonzero only in the presence of isoflurane.

Effects on α_1 and α_2, in the absence of changes in voltage dependence, indicate reduced conformational chemical potential energy between associated kinetic states. To estimate the magnitude of this effect, we calculated changes in the free energy barriers induced by isoflurane (ΔG_{ISO}; Fig. 6, left, insets). ΔG_{ISO} for rate constants was similar across channel types. ΔG_{ISO} for α_2 was approximately −0.7 kcal/mol, which is nearly fourfold greater than for α_1 (approximately −0.2 kcal/mol). These results indicate that isoflurane primarily reduces the chemical potential energy barrier of inactivation (α_2) and, to a lesser degree, activation (α_1).

DISCUSSION

We combined electrophysiological and kinetic modeling studies to reveal several novel mechanistic insights into isoflurane modulation of NaChBac function. Isoflurane accelerated both activation and inactivation kinetics and shifted activation and SSI relationships to more hyperpolarized potentials without slowing recovery from inactivation. To provide insight into structure–function relationships and the possibility of slow open channel block, we studied two channel mutations, G229A and G219A, which inhibit or enhance inactivation, respectively. A six-state NaChBac gating model (Kuzmenkin et al., 2004) was used to analyze macroscopic gating to estimate underlying microscopic gating. This model was sufficient to quantitatively account for gating in the absence or presence of isoflurane, thus arguing against the importance of slow open channel block. The results indicate that isoflurane modulation of NaChBac involves enhancement of microscopic activation and inactivation without stabilization of the inactivated state at resting membrane potentials.

Enhancement of NaChBac activation by isoflurane

Isoflurane increased the microscopic activation rate constant (α_1) and induced a hyperpolarized shift of the *G-V* relationship in WT NaChBac, in agreement with results for sevoflurane, a related ether anesthetic, on NaChBac (Barber et al., 2014). Similar hyperpolarized shifts in *G-V* relationships have been reported for sevoflurane on Shaker-type voltage-gated potassium channels (Barber et al., 2012; Liang et al., 2015) but were not found in a previous study of isoflurane effects on NaChBac (Ouyang et al., 2007), probably because of the use of a different voltage protocol (see last paragraph, this section). These effects were also observed in G219A, but with smaller hyperpolarizing *G-V* shifts compared with WT. G229A manifested increased α_1 but lacked a significant shift in the *G-V* relationship.

Isoflurane reduced the chemical potential energy barrier of activation of all channels to similar degree ($k_{\alpha 1}(0)$, $\Delta G_{ISO} \approx -0.2$ kcal/mol), indicating that the G219A and G229A mutations do not alter the mechanism underlying the isoflurane effect. The voltage dependence of activation was little changed by isoflurane, with the possible exception of G219A. Isoflurane also raised α_1, with absolute increases more than 10-fold greater than for α_2. Small but significant leftward shifts in *G-V* relationships might simply be caused by greater peak open probability at a particular voltage arising from a disproportionately larger absolute increase in channel opening rates relative to inactivation. In this case, increases in the absolute channel opening rate that are unmatched by those of closing rates (inactivation) can lead to increased peak open channel probability. A related possibility is that changes in macroscopic activa-
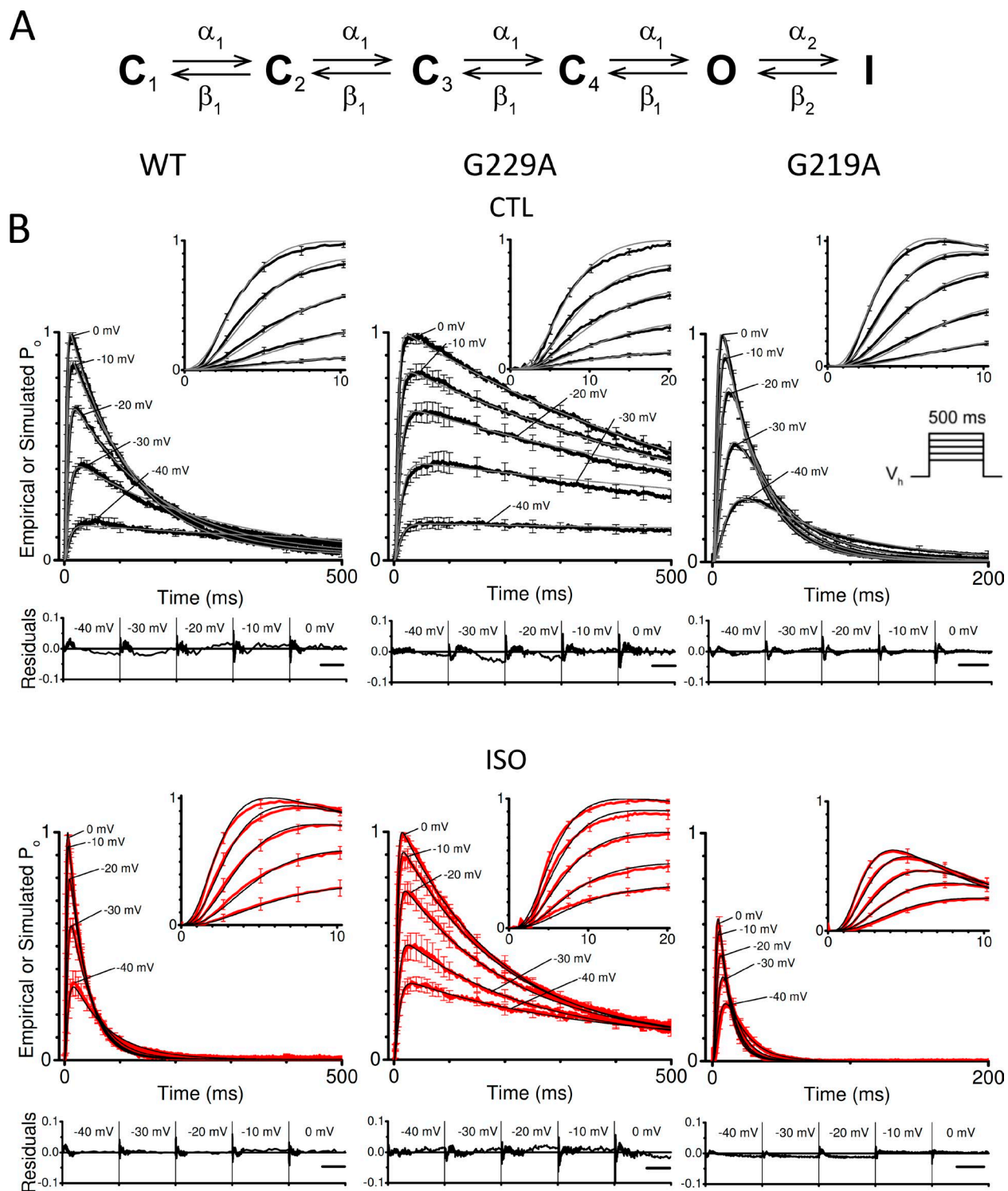
Figure 5. Fitting of NaChBac current responses using the six-state Markov model. (A) A sequential six-state Markov model proposed by Kuzmenkin et al. (2004) to account for NaChBac gating based on ionic and gating current results. Four closed states (C_n) are visited as governed by forward (α_1) and backward (β_1) rate constants before the open state (O). O transitions to the inactivated state (I) governed by forward (α_2) and backward (β_2) rate constants. (B) The six-state model was used to analyze isoflurane microscopic gating effects manifest in families of mean (±SEM; $n = 4$–6) normalized P_o responses (empirical, coarse black and red lines) over a range of triggering voltages (−40 to 0 mV, voltage protocol shown in top, left, bottom inset) in control (top) and 0.8 mM isoflurane (bottom) for each channel as indicated. The fitted six-state model P_o responses (simulated, smooth gray and black lines) reproduced mean normalized P_o responses, including the activation phase (top insets), where "goodness of fit" is supported by residual plots (bottom, time bars 200 ms, 200 ms, and 100 ms for WT, G229A, and G219A, respectively). Optimal model parameter

Isoflurane modulates NaChBac gating | Sand et al.

tion induced by isoflurane arise strictly from alterations of inactivation. We explored this possibility by fixing activation rate constants (α_1 and β_1) and reestimating the resultant parameter subset in the presence of isoflurane. Model responses (unpublished data) did not account for the activation phase upon visual inspection, and *F*-test analysis indicated that the fit was statistically better when activation rate constants were estimated ($P < 0.05$), thereby supporting changes in activation.

Ouyang et al. (2007) reported that isoflurane reduced WT NaChBac peak currents, in contrast to the results of this study. This divergent result can be explained by differences in the holding potential used. We used holding potentials of -140 and -160 mV to minimize the fraction of inactivated channels. In contrast, Ouyang et al. (2007) analyzed the effects of isoflurane at more depolarized membrane potentials (-80 mV). Our WT SSI curve indicates that at a holding potential of -80 mV the predicted fraction of inactivated channels is $\sim$0.2, and this fraction is promoted by isoflurane. Under these conditions, isoflurane depressed peak current, but based on our current findings this result likely arose from the presence of a significant fraction of inactivated channels induced by the depolarized holding potentials and isoflurane.

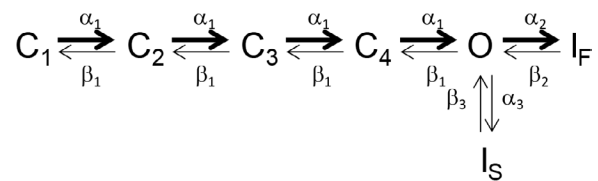### Isoflurane effects on NaChBac inactivation

Isoflurane increased the inactivation rate constant (α_2) for all channels and induced a hyperpolarized shift of SSI in WT and G219A, with the effect on G229A unknown. Isoflurane also accelerated recovery from inactivation in WT channels at resting membrane potentials, similar to sevoflurane effects (Barber et al., 2014). This effect was not evident in the six-state kinetic model, which showed no statistical effect of isoflurane on the parameter β_2 at depolarized potentials. Isoflurane reduced the chemical potential energy barrier for inactivation of all channels to a similar degree ($k_{\alpha2}(0)$, $\Delta G_{ISO} \approx -0.7$ kcal/mol), indicating that the mutations do not alter the mechanism of this isoflurane effect. This effect is fourfold greater than for α_1, making this the predominant effect of isoflurane on channel gating. For all channels, α_2 exhibited little voltage dependence in control as reported by z_2 and x_2 values, consistent with voltage modulation of macroscopic inactivation being determined solely by changes in open channel probability (Aldrich et al., 1983).

Recovery from inactivation in WT channels after 500-ms depolarizations was biexponential, with fast ($\tau_F \approx 50$ ms) and slow ($\tau_S \approx 350$ ms) components. The kinetics of the slow component are consistent with a previous study

involving longer depolarizations (Ren et al., 2001). Our results indicate two forms of inactivation, slow and fast, with the fast component dominant in our experimental protocols, and likely accounting for the observed monoexponential macroscopic inactivation time course. Isoflurane accelerated overall recovery from inactivation by increasing the fraction of the fast component at the expense of the slow without altering individual recovery time constants, suggesting that isoflurane selectively promotes the fast inactivated state. These findings are not easily explained by a simple open block mechanism.

Proposed allosteric model of isoflurane modulation of NaChBac

We probed the pharmacologic mechanisms underlying isoflurane modulation of NaChBac using a six-state Markov NaChBac model based on gating current and charge movement results and validated by reconciling macroscopic currents (Kuzmenkin et al., 2004). Optimal estimated rate constants allowed the six-state model to reproduce channel gating over a range of potentials for all channels, in the absence or presence of isoflurane (Scheme 2):

$$C_1 \underset{\beta_1}{\overset{\alpha_1}{\rightleftharpoons}} C_2 \underset{\beta_1}{\overset{\alpha_1}{\rightleftharpoons}} C_3 \underset{\beta_1}{\overset{\alpha_1}{\rightleftharpoons}} C_4 \underset{\beta_1}{\overset{\alpha_1}{\rightleftharpoons}} O \underset{\beta_2}{\overset{\alpha_2}{\rightleftharpoons}} I_F$$
$$\beta_3 \updownarrow \alpha_3$$
$$I_S$$

(Scheme 2)

Scheme 2 represents our proposed allosteric mechanism of isoflurane modulation of WT NaChBac. This model is an extension of the model proposed by Kuzmenkin et al. (2004) (Scheme 1). The additional features of Scheme 2 are based on direct empirical observations as well as those arising from the analysis of empirical results using Scheme 1. The structure of the activation/inactivation backbone is unchanged; the bolded α_1 and α_2 transition arrows signify isoflurane enhancement in accord with our findings. The preexisting inactivated state *I* has been relabeled the fast inactivated state I_F, and a second slow inactivated state (I_S) has been introduced with associated inactivation and recovery rate constants α_3 and β_3, respectively. These revisions reconcile biexponential recovery from inactivation at resting membrane potentials in which isoflurane promotes I_F at the expense of I_S without changing recovery time constants. Analysis of the biexponential

sets were estimated using the entire voltage family of mean normalized P_o responses as targets (see Materials and methods). Top insets show responses replotted on an expanded timescale to focus on the early activation time course. Below are serial presentations of associated fit residual plots at the indicated voltages.
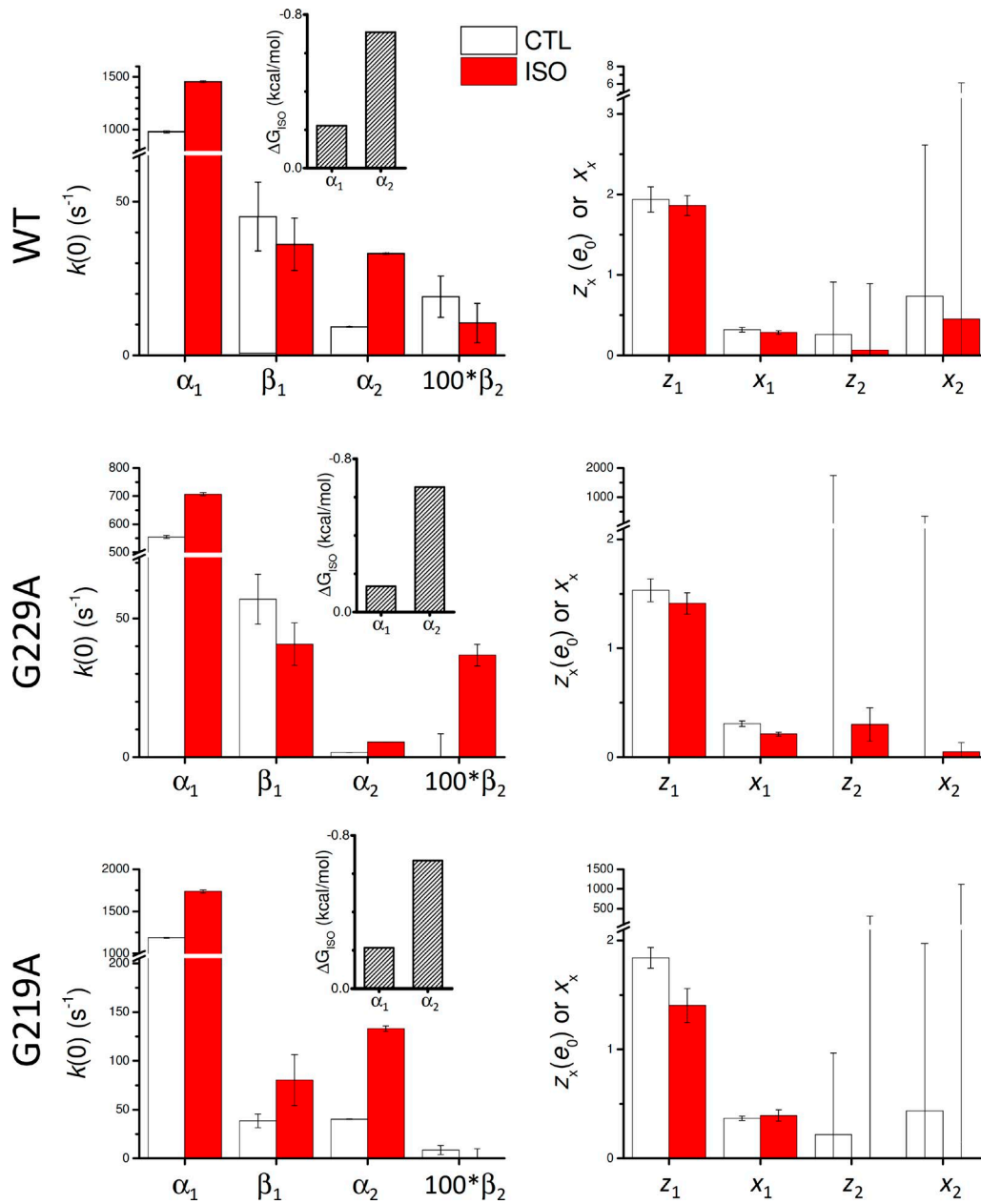
Figure 6. **Isoflurane effects on NaChBac gating parameters analyzed using the six-state Markov model.** Plots of estimated gating parameters with 95% confidence intervals for $k_x(0)$ of rate constants (left) and z_x and x_x (right). Parameter estimation involved fitting model P_o responses to one family of mean normalized P_o responses for each experimental condition (see Fig. 5). 95% confidence intervals were determined for the final value of each estimated parameter. Negative confidence intervals were limited to zero. β_2 values were scaled up by 100 for clarity because values were uniformly less than one. Insets show estimated change in free energy of associated gating transition (ΔG_{ISO}) induced by isoflurane (see Materials and methods). Estimated values with 95% confidence interval of model parameters $k_{\alpha1}(0)$, $k_{\beta1}(0)$, $k_{\alpha2}(0)$, $k_{\beta2}(0)$ (s^{-1}) and z_1, x_1, z_2, x_2 (z_x[e0] and x_x [unitless]) are as follows: WT CTL: 978 ± 9.2, 45.1 ± 11.1, 9.33 ± 0.14, 0.19 ± 0.068, 1.94 ± 0.16, 0.32 ± 0.028, 0.26 ± 0.65, 0.74 ± 1.87; ISO: 1,450 ± 9.9, 36.1 ± 8.5, 33.1 ± 0.28, 0.11 ± 0.064, 1.86 ± 0.12, 0.29 ± 0.02, 0.067 ± 0.83, 0.45 ± 5.67; G229A CTL: 555 ± 5.13, 56.9 ± 8.9, 1.69 ± 0.048, 1.01 × 10^{-6} ± 0.084, 1.53 ± 0.10, 0.31 ± 0.025, 4.7 × 10^{-4} ± 2,700, 5.8 × 10^{-5} ± 354; ISO: 707 ± 5.25, 40.7 ± 7.7, 5.42 ± 0.075, 36.8 ± 3.8, 1.41 ± 0.094, 0.21 ± 0.017, 0.3 ± 0.15, 0.046 ± 0.088; G219A CTL: 1,190 ± 7.72, 38.5 ± 6.84, 40.3 ± 0.33, 8.77 ± 4.62, 1.84 ± 0.093, 0.37 ± 0.021, 0.22 ± 0.75, 0.44 ± 1.53; ISO: 1,740 ± 19.1, 80.4 ± 26.1, 133 ± 2.87, 0.039 ± 9.81, 1.4 ± 0.17, 0.39 ± 0.049, 4.2 × 10^{-6} ± 302, 6.7 × 10^{-5} ± 1,110, respectively. Estimated values with 95% confidence intervals of model scale factors K_{-40mV}, K_{-30mV}, K_{-20mV}, K_{-10mV}, and K_{0mV} are as follows: WT CTL: 0.91 ± 0.1, 0.86 ± 0.05, 0.94 ± 0.05, 1.12 ± 0.03, 1.18 ± 0.02; ISO: 0.82 ± 0.04, 0.98 ± 0.02, 1.09 ± 0.02, 1.17 ± 0.02, 1.18 ± 0.02; G229A CTL: 1.13 ± 0.14, 1.03 ± 0.06, 0.98 ± 0.04, 0.99 ± 0.02, 1.07 ± 0.02; ISO: 0.82 ± 0.04, 0.85 ± 0.02, 0.94 ± 0.02, 1.05 ± 0.02, 1.09 ± 0.02; G219A CTL: 0.91 ± 0.04, 1.03 ± 0.05, 1.07 ± 0.02, 1.13 ± 0.02, 1.17 ± 0.02; ISO: 0.87 ± 0.06, 0.85 ± 0.06, 0.88 ± 0.05, 0.937 ± 0.04, 0.93 ± 0.02, respectively.

Isoflurane modulates NaChBac gating | Sand et al.

recovery from inactivation provides quantitative insight into β_2 and β_3 at polarized membrane potentials (-140 mV). The WT SSI curve (Fig. 3 C) indicates that a membrane potential of -140 mV returns all channels to a resting available state over time. Therefore, forward inactivation rates (α_2 and α_3) can be considered negligible relative to the corresponding backward rates (β_2 and β_3). In light of this reasoning, the coefficients of the biexponential function then reflect the relative probabilities of I_S and I_F at the end of the conditioning pulse, and time constants report reciprocal values of recovery rate constants (β_2 and β_3). Therefore, recovery inactivation rate constants were calculated for WT control ($\beta_2 = 21.3$ s^{-1}, $\beta_3 = 3.13$ s^{-1}), which are changed little by isoflurane. The unbolded α_3, β_1, β_2, and β_3 transition arrows indicate no isoflurane modulation. At depolarized potentials (-40 to 0 mV), estimated values of β_2 are more than 20-fold smaller than α_2, supporting the proposal that I_F is nearly absorbing in this voltage range.

Open channel block of NaChBac by isoflurane

Barber et al. (2014) proposed a mechanism for sevoflurane modulation of WT NaChBac that involves open channel block based on results from molecular dynamics simulations. The simulations showed sevoflurane in the channel pore interacting with conserved NaChBac residues (T220 and F227), in which homologous residues in mammalian Na$_v$ play critical roles in local anesthetic (LA) pore block of open channels. Further support came from extension of the six-state NaChBac gating model (Kuzmenkin et al., 2004) to include a slow open channel block mechanism. The slow open channel block model semi-quantitatively accounted for some of isoflurane effects, including acceleration of macroscopic inactivation, hyperpolarizing shifts of G-V and SSI relationships, and accelerated recovery from apparent inactivation at resting membrane potentials.

Although a pore-blocking mechanism by neutral isoflurane is possible, it is unlikely that isoflurane pharmacology parallels that of charged LA open channel block. Most LAs exhibit uncharged and charged states (tertiary and quaternary amines) at physiological pH in which the charged form participates in high-affinity open channel pore binding, and such block is mediated by F1579 (Na$_v$1.4; Kimbrough and Gingrich, 2000), homologous to F227 in NaChBac. Recent ^{19}F NMR binding data show very weak interactions between isoflurane and F227 in NaChBac (Kinde et al., 2016). Furthermore, high-affinity intrapore LA binding is mediated by cation-π binding involving the charged LA head and F1579 aromatic ring (Ahern et al., 2008).

To further explore the ability of a simple open channel block to account for isoflurane effects on NaChBac, we extended our Scheme 1 to include an open channel blocked state (B) as proposed by Barber et al. (2014) (their Fig. 4 B). Those authors reported sevoflurane-induced increases in β_2, in contrast to our finding that β_2 was little changed. We next estimated all parameters to include those associated with open channel block (K_{on} and K_{off}). Given our empirical target dataset for WT NaChBac, inclusion of an open block mechanism led to reduced peak open probability (with K_{on} limited to nonzero positive values), a slight change in β_2, and a value of K_{off} that approached zero. The effects of increased β_2 and a nonzero K_{off} both promote open state probability because they mediate channel reopening from nonconducting states I and B, which leads to incomplete inactivation and a visible I_{Na} plateau. An I_{Na} plateau was observed in simulations by Barber et al. (2014) (their Fig. 4 C), but this observation is absent in representative current time courses (their Fig. 3, A and C) as well as in our empirical results (Fig. 5 B, left). A recent NMR binding study identified a strong isoflurane binding site at the base of the selectivity filter at residue T189, which lies at the extracellular mouth of the pore (Kinde et al., 2016), leading those authors to postulate that isoflurane binds at this site to occlude ion conduction. However, our data and kinetic modeling results do not favor an open channel blocking mechanism for isoflurane modulation of NaChBac.

Structural basis for allosteric modulation of NaChBac by isoflurane

NaChBac appears to manifest only slow or C-type–like inactivation (Catterall, 2001; Pavlov et al., 2005) that is similar to that of eukaryotic Na$_v$ (Ong et al., 2000; Vilin and Ruben, 2001). Slow inactivation is thought to involve the P-loops in eukaryotic channels (Ong et al., 2000; Vilin and Ruben, 2001) as well as in prokaryotic channels such as NaChBac (Pavlov et al., 2005). Specifically, a collapse of the selectivity filter is thought to underlie prokaryotic Na$^+$ channel inactivation (for review, see Bagnéris et al., 2015). Sevoflurane and isoflurane were predicted through molecular dynamics simulations to bind to residues in the NaChBac P-loops (Raju et al., 2013; Barber et al., 2014). Two of these interactions were recently confirmed by ^{19}F NMR studies (Kinde et al., 2016), in which isoflurane had strong interactions with T189 at the base of the selectivity filter and S208, an extracellular residue connecting the P2 loop to the S6 helix. The isoflurane binding site at the base of the selectivity filter might represent a distinct binding site governing effects on NaChBac inactivation, similar to that proposed for LA modulation of slow inactivation in Na$_v$1.4 (Chen et al., 2000).

Charged residues in S4 contribute to the NaChBac voltage sensor (Chahine et al., 2004; Blanchet et al., 2007), and in S5–S6 contribute to the permeation pore (Yue et al., 2002). S4 voltage sensor movements trigger pore opening involving the S4–S5 linker, which has been predicted as a site of action for volatile general anesthetics for both NaChBac (Raju et al., 2013; Barber

et al., 2014) and voltage-gated potassium channels (Barber et al., 2011; Liang et al., 2015). The S4–S5 linker was also identified as an isoflurane binding site by ^{19}F NMR, with isoflurane interacting strongly with S129 (Kinde et al., 2016). This leads us to speculate that the S4–S5 linker represents a second isoflurane binding site that selectively governs anesthetic effects on activation. Alternatively, the extracellular binding site at S208 could also be involved, as it connects the pore loops with S6 and could thus influence the rigid-body motions of the activation gate (Kinde et al., 2016). Site-directed mutagenesis of these two putative sites with electrophysiological characterization of activation kinetics might answer this question.

Limitations

The validity of our kinetic modeling relied on the fitting of current families from the same cell before and after exposure to isoflurane. Because of the slow kinetic properties of NaChBac, it was not feasible to collect data using multiple electrophysiological protocols during the course of one experiment without compromising preparation stability. Therefore, although it would have been ideal to simultaneously model current families from deactivation, SSI, or recovery protocols, we focused on the analysis of currents resulting from depolarizing steps. This necessarily highlights changes to forward rate constants, which are accelerating under these conditions, and may not reveal more subtle effects on backward rate constants. The faster kinetics of mammalian Na$_v$ would permit more detailed analysis in this regard.

Mammalian Na$_v$ isoforms manifest both fast and slow forms of inactivation, and isoflurane enhances Na$_v$1.2 fast inactivation (Purtell et al., 2015). Even so, bacterial Na$^+$ channels have structural similarities to mammalian Na$_v$ that support their use as experimental models (Bagnéris et al., 2014; Catterall and Zheng, 2015; Payandeh and Minor, 2015). Recent computational studies using bacterial Na$^+$ channel crystal structures reveal similarities in the outer pore (Tikhonov and Zhorov, 2012; Korkosh et al., 2014; Lukacs et al., 2014; Mahdavi and Kuyucak, 2014) and pore fenestrations (Kaczmarski and Corry, 2014). Moreover, the presence of slow inactivation in mammalian Na$_v$ highlights the utility of our results. Drug modulation of Na$_v$ slow inactivation is important in treating neuropathic pain, arrhythmias, and epilepsy (Remy et al., 2004; Lenkowski et al., 2007; Errington et al., 2008) and is involved in neuronal plasticity (Vilin and Ruben, 2001). Further studies are required to examine anesthetic effects on slow inactivation in mammalian Na$_v$ and expand investigation to other channel states, examine single-channel effects, and determine whether isoflurane and sevoflurane have conserved mechanisms of action.

Conclusions

We find that isoflurane reduces Na$^+$ currents through NaChBac by increasing both forward activation and inactivation rate constants. These effects likely result from multiple sites of isoflurane interaction with the channel. Mutagenesis and structural modeling will be required to test the S4–S5 linker residue S129 and the extracellular P-loop residue S208 as putative anesthetic binding sites mediating effects on activation and the role of the T189 binding site in modulating inactivation. This work provides a biophysical and structural framework to guide further structural studies and facilitate the design of more effective and safer general anesthetics.

REFERENCES

Ahern, C.A., A.L. Eastwood, D.A. Dougherty, and R. Horn. 2008. Electrostatic contributions of aromatic residues in the local anesthetic receptor of voltage-gated sodium channels. *Circ. Res.* 102:86–94. http://dx.doi.org/10.1161/CIRCRESAHA.107.160663

Aldrich, R.W., D.P. Corey, and C.F. Stevens. 1983. A reinterpretation of mammalian sodium channel gating based on single channel recording. *Nature.* 306:436–441. http://dx.doi.org/10.1038/306436a0

Bagnéris, C., P.G. DeCaen, C.E. Naylor, D.C. Pryde, I. Nobeli, D.E. Clapham, and B.A. Wallace. 2014. Prokaryotic NavMs channel as a structural and functional model for eukaryotic sodium channel antagonism. *Proc. Natl. Acad. Sci. USA.* 111:8428–8433. http://dx.doi.org/10.1073/pnas.1406855111

Bagnéris, C., C.E. Naylor, E.C. McCusker, and B.A. Wallace. 2015. Structural model of the open-closed-inactivated cycle of prokaryotic voltage-gated sodium channels. *J. Gen. Physiol.* 145:5–16. http://dx.doi.org/10.1085/jgp.201411242

Barber, A.F., Q. Liang, C. Amaral, W. Treptow, and M. Covarrubias. 2011. Molecular mapping of general anesthetic sites in a voltage-gated ion channel. *Biophys. J.* 101:1613–1622. http://dx.doi.org/10.1016/j.bpj.2011.08.026

Barber, A.F., Q. Liang, and M. Covarrubias. 2012. Novel activation of voltage-gated K$^+$ channels by sevoflurane. *J. Biol. Chem.* 287:40425–40432. http://dx.doi.org/10.1074/jbc.M112.405787

Barber, A.F., V. Carnevale, M.L. Klein, R.G. Eckenhoff, and M. Covarrubias. 2014. Modulation of a voltage-gated Na+ channel by sevoflurane involves multiple sites and distinct mechanisms. *Proc. Natl. Acad. Sci. USA*. 111:6726–6731. http://dx.doi.org/10.1073/pnas.1405768111

Blanchet, J., S. Pilote, and M. Chahine. 2007. Acidic residues on the voltage-sensor domain determine the activation of the NaChBac sodium channel. *Biophys. J.* 92:3513–3523. http://dx.doi.org/10.1529/biophysj.106.090464

Catterall, W.A. 2001. Physiology. A one-domain voltage-gated sodium channel in bacteria. *Science*. 294:2306–2308. http://dx.doi.org/10.1126/science.1067417

Catterall, W.A., and N. Zheng. 2015. Deciphering voltage-gated Na$^+$ and Ca^{2+} channels by studying prokaryotic ancestors. *Trends Biochem. Sci.* 40:526–534. http://dx.doi.org/10.1016/j.tibs.2015.07.002

Chahine, M., S. Pilote, V. Pouliot, H. Takami, and C. Sato. 2004. Role of arginine residues on the S4 segment of the *Bacillus halodurans* Na$^+$ channel in voltage-sensing. *J. Membr. Biol.* 201:9–24. http://dx.doi.org/10.1007/s00232-004-0701-z

Chen, Z., B.H. Ong, N.G. Kambouris, E. Marbán, G.F. Tomaselli, and J.R. Balser. 2000. Lidocaine induces a slow inactivated state in rat skeletal muscle sodium channels. *J. Physiol.* 524:37–49. http://dx.doi.org/10.1111/j.1469-7793.2000.t01-1-00037.x

Errington, A.C., T. Stöhr, C. Heers, and G. Lees. 2008. The investigational anticonvulsant lacosamide selectively enhances slow inactivation of voltage-gated sodium channels. *Mol. Pharmacol.* 73:157–169. http://dx.doi.org/10.1124/mol.107.039867

Eyring, H. 1935. The activation complex in chemical reactions. *J. Chem. Phys.* 3:107–115. http://dx.doi.org/10.1063/1.1749604

Franks, N.P. 2006. Molecular targets underlying general anaesthesia. *Br. J. Pharmacol.* 147:S72–S81. http://dx.doi.org/10.1038/sj.bjp.0706441

Hemmings, H.C. Jr., M.H. Akabas, P.A. Goldstein, J.R. Trudell, B.A. Orser, and N.L. Harrison. 2005. Emerging molecular mechanisms of general anesthetic action. *Trends Pharmacol. Sci.* 26:503–510. http://dx.doi.org/10.1016/j.tips.2005.08.006

Herold, K.F., and H.C. Hemmings Jr. 2012. Sodium channels as targets for volatile anesthetics. *Front. Pharmacol.* 3:50. http://dx.doi.org/10.3389/fphar.2012.00050

Herold, K.F., C. Nau, W. Ouyang, and H.C. Hemmings Jr. 2009. Isoflurane inhibits the tetrodotoxin-resistant voltage-gated sodium channel Na$_v$1.8. *Anesthesiology*. 111:591–599. http://dx.doi.org/10.1097/ALN.0b013e3181af64d4

Herold, K.F., R.L. Sanford, W. Lee, M.F. Schultz, H.I. Ingólfsson, O.S. Andersen, and H.C. Hemmings Jr. 2014. Volatile anesthetics inhibit sodium channels without altering bulk lipid bilayer properties. *J. Gen. Physiol.* 144:545–560. http://dx.doi.org/10.1085/jgp.201411172

Herold, K.F., R.L. Sanford, W. Lee, O.S. Andersen, and H.C. Hemmings Jr. 2017. Clinical concentrations of chemically diverse general anesthetics minimally affect lipid bilayer properties. *Proc. Natl. Acad. Sci. USA*. 114:3109–3114. http://dx.doi.org/10.1073/pnas.1611717114

Irie, K., K. Kitagawa, H. Nagura, T. Imai, T. Shimomura, and Y. Fujiyoshi. 2010. Comparative study of the gating motif and C-type inactivation in prokaryotic voltage-gated sodium channels. *J. Biol. Chem.* 285:3685–3694. http://dx.doi.org/10.1074/jbc.M109.057455

Kaczmarski, J.A., and B. Corry. 2014. Investigating the size and dynamics of voltage-gated sodium channel fenestrations: A molecular dynamics study. *Channels (Austin)*. 8:264–277. http://dx.doi.org/10.4161/chan.28136

Kimbrough, J.T., and K.J. Gingrich. 2000. Quaternary ammonium block of mutant Na$^+$ channels lacking inactivation: Features of a transition-intermediate mechanism. *J. Physiol.* 529:93–106. http://dx.doi.org/10.1111/j.1469-7793.2000.00093.x

Kinde, M.N., V. Bondarenko, D. Granata, W. Bu, K.C. Grasty, P.J. Loll, V. Carnevale, M.L. Klein, R.G. Eckenhoff, P. Tang, and Y. Xu. 2016. Fluorine-19 NMR and computational quantification of isoflurane binding to the voltage-gated sodium channel NaChBac. *Proc. Natl. Acad. Sci. USA*. 113:13762–13767. http://dx.doi.org/10.1073/pnas.1609939113

Korkosh, V.S., B.S. Zhorov, and D.B. Tikhonov. 2014. Folding similarity of the outer pore region in prokaryotic and eukaryotic sodium channels revealed by docking of conotoxins GIIIA, PIIIA, and KIIIA in a Na$_v$Ab-based model of Na$_v$1.4. *J. Gen. Physiol.* 144:231–244. http://dx.doi.org/10.1085/jgp.201411226

Kuzmenkin, A., F. Bezanilla, and A.M. Correa. 2004. Gating of the bacterial sodium channel, NaChBac: Voltage-dependent charge movement and gating currents. *J. Gen. Physiol.* 124:349–356. http://dx.doi.org/10.1085/jgp.200409139

Lenkowski, P.W., T.W. Batts, M.D. Smith, S.H. Ko, P.J. Jones, C.H. Taylor, A.K. McCusker, G.C. Davis, H.A. Hartmann, H.S. White, et al. 2007. A pharmacophore derived phenytoin analogue with increased affinity for slow inactivated sodium channels exhibits a desired anticonvulsant profile. *Neuropharmacology*. 52:1044–1054. http://dx.doi.org/10.1016/j.neuropharm.2006.11.001

Liang, Q., W.D. Anderson, S.T. Jones, C.S. Souza, J.M. Hosoume, W. Treptow, and M. Covarrubias. 2015. Positive allosteric modulation of Kv channels by sevoflurane: Insights into the structural basis of inhaled anesthetic action. *PLoS One*. 10:e0143363. http://dx.doi.org/10.1371/journal.pone.0143363

Lukacs, P., V.S. Gawali, R. Cervenka, S. Ke, X. Koenig, L. Rubi, T. Zarrabi, K. Hilber, A. Stary-Weinzinger, and H. Todt. 2014. Exploring the structure of the voltage-gated Na$^+$ channel by an engineered drug access pathway to the receptor site for local anesthetics. *J. Biol. Chem.* 289:21770–21781. http://dx.doi.org/10.1074/jbc.M113.541763

Mahdavi, S., and S. Kuyucak. 2014. Molecular dynamics study of binding of μ-conotoxin GIIIA to the voltage-gated sodium channel Na$_v$1.4. *PLoS One*. 9:e105300. http://dx.doi.org/10.1371/journal.pone.0105300

McCusker, E.C., C. Bagnéris, C.E. Naylor, A.R. Cole, N. D'Avanzo, C.G. Nichols, and B.A. Wallace. 2012. Structure of a bacterial voltage-gated sodium channel pore reveals mechanisms of opening and closing. *Nat. Commun.* 3:1102. http://dx.doi.org/10.1038/ncomms2077

Ong, B.H., G.F. Tomaselli, and J.R. Balser. 2000. A structural rearrangement in the sodium channel pore linked to slow inactivation and use dependence. *J. Gen. Physiol.* 116:653–662. http://dx.doi.org/10.1085/jgp.116.5.653

OuYang, W., and H.C. Hemmings Jr. 2007. Isoform-selective effects of isoflurane on voltage-gated Na$^+$ channels. *Anesthesiology*. 107:91–98. http://dx.doi.org/10.1097/01.anes.0000268390.28362.4a

Ouyang, W., T.Y. Jih, T.T. Zhang, A.M. Correa, and H.C. Hemmings Jr. 2007. Isoflurane inhibits NaChBac, a prokaryotic voltage-gated sodium channel. *J. Pharmacol. Exp. Ther.* 322:1076–1083. http://dx.doi.org/10.1124/jpet.107.122929

Ouyang, W., K.F. Herold, and H.C. Hemmings Jr. 2009. Comparative effects of halogenated inhaled anesthetics on voltage-gated Na$^+$ channel function. *Anesthesiology*. 110:582–590. http://dx.doi.org/10.1097/ALN.0b013e318197941e

Pavlov, E., C. Bladen, R. Winkfein, C. Diao, P. Dhaliwal, and R.J. French. 2005. The pore, not cytoplasmic domains, underlies inactivation in a prokaryotic sodium channel. *Biophys. J.* 89:232–242. http://dx.doi.org/10.1529/biophysj.104.056994

Payandeh, J., and D.L. Minor Jr. 2015. Bacterial voltage-gated sodium channels (BacNa$_V$s) from the soil, sea, and salt lakes enlighten molecular mechanisms of electrical signaling and pharmacology in the brain and heart. *J. Mol. Biol.* 427:3–30. http://dx.doi.org/10.1016/j.jmb.2014.08.010

Payandeh, J., T. Scheuer, N. Zheng, and W.A. Catterall. 2011. The crystal structure of a voltage-gated sodium channel. *Nature.* 475:353–358. http://dx.doi.org/10.1038/nature10238

Payandeh, J., T.M. Gamal El-Din, T. Scheuer, N. Zheng, and W.A. Catterall. 2012. Crystal structure of a voltage-gated sodium channel in two potentially inactivated states. *Nature.* 486:135–139.

Purtell, K., K.J. Gingrich, W. Ouyang, K.F. Herold, and H.C. Hemmings Jr. 2015. Activity-dependent depression of neuronal sodium channels by the general anaesthetic isoflurane. *Br. J. Anaesth.* 115:112–121. http://dx.doi.org/10.1093/bja/aev203

Raju, S.G., A.F. Barber, D.N. LeBard, M.L. Klein, and V. Carnevale. 2013. Exploring volatile general anesthetic binding to a closed membrane-bound bacterial voltage-gated sodium channel via computation. *PLOS Comput. Biol.* 9:e1003090. http://dx.doi.org/10.1371/journal.pcbi.1003090

Rehberg, B., Y.H. Xiao, and D.S. Duch. 1996. Central nervous system sodium channels are significantly suppressed at clinical concentrations of volatile anesthetics. *Anesthesiology.* 84:1223–1233. http://dx.doi.org/10.1097/00000542-199605000-00025

Remy, C., S. Remy, H. Beck, D. Swandulla, and M. Hans. 2004. Modulation of voltage-dependent sodium channels by the delta-agonist SNC80 in acutely isolated rat hippocampal neurons. *Neuropharmacology.* 47:1102–1112. http://dx.doi.org/10.1016/j.neuropharm.2004.06.034

Ren, D., B. Navarro, H. Xu, L. Yue, Q. Shi, and D.E. Clapham. 2001. A prokaryotic voltage-gated sodium channel. *Science.* 294:2372–2375. http://dx.doi.org/10.1126/science.1065635

Shaya, D., F. Findeisen, F. Abderemane-Ali, C. Arrigoni, S. Wong, S.R. Nurva, G. Loussouarn, and D.L. Minor Jr. 2014. Structure of a prokaryotic sodium channel pore reveals essential gating elements and an outer ion binding site common to eukaryotic channels. *J. Mol. Biol.* 426:467–483. http://dx.doi.org/10.1016/j.jmb.2013.10.010

Shiraishi, M., and R.A. Harris. 2004. Effects of alcohols and anesthetics on recombinant voltage-gated Na+ channels. *J. Pharmacol. Exp. Ther.* 309:987–994. http://dx.doi.org/10.1124/jpet.103.064063

Taheri, S., M.J. Halsey, J. Liu, E.I. Eger II, D.D. Koblin, and M.J. Laster. 1991. What solvent best represents the site of action of inhaled anesthetics in humans, rats, and dogs? *Anesth. Analg.* 72:627–634. http://dx.doi.org/10.1213/00000539-199105000-00010

Tikhonov, D.B., and B.S. Zhorov. 2012. Architecture and pore block of eukaryotic voltage-gated sodium channels in view of Na$_V$Ab bacterial sodium channel structure. *Mol. Pharmacol.* 82:97–104. http://dx.doi.org/10.1124/mol.112.078212

Vilin, Y.Y., and P.C. Ruben. 2001. Slow inactivation in voltage-gated sodium channels: Molecular substrates and contributions to channelopathies. *Cell Biochem. Biophys.* 35:171–190. http://dx.doi.org/10.1385/CBB:35:2:171

Yue, L., B. Navarro, D. Ren, A. Ramos, and D.E. Clapham. 2002. The cation selectivity filter of the bacterial sodium channel, NaChBac. *J. Gen. Physiol.* 120:845–853. http://dx.doi.org/10.1085/jgp.20028699

Zhang, X., W. Ren, P. DeCaen, C. Yan, X. Tao, L. Tang, J. Wang, K. Hasegawa, T. Kumasaka, J. He, et al. 2012. Crystal structure of an orthologue of the NaChBac voltage-gated sodium channel. *Nature.* 486:130–134.